

Article

Inversion of Nighttime PM_{2.5} Mass Concentration in Beijing Based on the VIIRS Day-Night Band

Xiaoran Zhao, Hanqing Shi *, Hong Yu and Pinglv Yang

Institute of Meteorology and Oceanography, PLA University of Science and Technology, Nanjing 211101, China; zhaoxiaoran_zxr@sina.com (X.Z.); nj_yuhong@aliyun.com (H.Y.); pl_yang@yahoo.com (P.Y.)

* Correspondence: lgdx_shi@sina.com; Tel.: +86-25-8083-0624

Academic Editors: Giovanni Pitari and Gabriele Curci

Received: 24 September 2016; Accepted: 14 October 2016; Published: 19 October 2016

Abstract: In order to monitor nighttime particular matter (PM) air quality in urban area, a back propagation neural network (BP neural network) inversion model is established, using low-light radiation data from the day/night band (DNB) of the Visible Infrared Imaging Radiometer Suite (VIIRS) aboard the Suomi National Polar-orbiting Partnership (S-NPP) satellite. The study focuses on the moonless and cloudless nights in Beijing during March–May 2015. A test is carried out by selecting surface PM_{2.5} data from 12 PM_{2.5} automatic monitoring stations and the corresponding night city light intensity from DNB. As indicated by the results, the linear correlation coefficient (R) between the results and the corresponding measured surface PM_{2.5} concentration is 0.91, and the root-mean-square error (RMSE) is 14.02 µg/m³ with the average of 59.39 µg/m³. Furthermore, the BP neural network model shows better accuracy when air relative humidity ranges from 40% to 80% and surface PM_{2.5} concentration exceeds 40 µg/m³. The study provides a superiority approach for monitoring PM_{2.5} air quality from space with visible light remote sensing data at night.

Keywords: low-light; nighttime PM_{2.5}; VIIRS/DNB; BP neural network

1. Introduction

PM_{2.5} refers to atmospheric particulates with aerodynamic diameters less than 2.5 µm in ambient air [1]. Although atmospheric particulates account for a small proportion of the particles in earth's atmosphere, they have an important impact on air quality, air visibility, atmosphere radiation balance, atmospheric photochemical reactions, and clouds and precipitation [2]. In comparison with coarse particulates in the atmosphere, due to a large surface area, PM_{2.5} can easily become carriers and reactants of other poisonous and hazardous substances. With the properties of long-distance transport and long-time retention in the atmosphere, PM_{2.5} can cause the damage to human health and ambient air conditions. PM_{2.5} mass concentration has become an important basis for evaluating ambient air quality. In 2012, a PM_{2.5} standard for ambient air was established in China; PM_{2.5} concentration limits were formally included into the National Ambient Air Quality Standard. The Level-I standard average annual and daily limits are specified at 15 µg/m³ and 35 µg/m³ respectively; the Level-II standard average annual and daily limits are specified at 35 µg/m³ and 75 µg/m³, respectively.

At present, means for monitoring PM_{2.5} mainly includes the Tapered Element Oscillating Microbalance (TEOM) method, β-ray method and light scattering method [3]. However, despite high measuring accuracy and continuity in time of ground-based observations, it is still difficult to implement large-range overall monitoring because of high instrument costs and a small coverage area. Along with the development of remote sensing technology, satellite remote sensing data has gradually been applied to the inversion of PM_{2.5}. Existing inversion methods mainly depend on Moderate Resolution Imaging Spectroradiometer (MODIS) aerosol optical depth (AOD) products [4–6], but MODIS products are only limited to daytime application, thus limiting the timeliness of PM_{2.5}

monitoring, and cannot carry out monitoring at night. Due to the limitation of nighttime visible sensor, there are few studies on nighttime $PM_{2.5}$ monitoring until the appearance of Operational Linear System (OLS) aboard the Defense Meteorological Satellite Program-Operational Linear System (DMSP) and Visible Infrared Imaging Radiometer Suite (VIIRS) aboard the Suomi National Polar-orbiting Partnership (S-NPP) satellite.

The S-NPP satellite, which launched in October 2011, is the first satellite of a new generation of National Polar-orbiting Operational Environmental Satellite System (NPOESS) Preparatory Project in the USA [7]. VIIRS inherits and develops a series of detection abilities of the Advanced Very High Resolution Radiometer (AVHRR) and MODIS. Particularly, VIIRS DNB has improved and optimized the low-light detection ability of the DMSP-OLS [8]. It can provide basic low-light sensitivities with the ability to see details in imagery at night.

Nighttime monitoring of $PM_{2.5}$ is of great significance in many aspects. First, as diurnal variation of $PM_{2.5}$ is characterized by significant periodicity, a more accurate diurnal variation of $PM_{2.5}$ could be acquired by combining nighttime monitoring results with daytime [9]. Second, factors leading to changes in $PM_{2.5}$ during dust-haze pollution have also obvious reaction at night such as relative humidity, temperature, wind speed and the nocturnal thermal inversion layer [10]. At the same time, motor vehicle exhaust, coal combustion, construction dust and secondary aerosols are also a main source of nighttime $PM_{2.5}$ [11]. The analysis of these factors will contribute to better understanding of the formation and dissipation rules of $PM_{2.5}$, and more rational formulation of control measures by relevant departments.

The potential of using VIIRS DNB for $PM_{2.5}$ air quality monitoring at night has been illustrated by researchers [12]. The application of advanced statistical models improves the correlation coefficient of ground-based measured $PM_{2.5}$ concentration and the derived $PM_{2.5}$ concentration [13]. However, meteorological elements also impact the air quality at night. In the present work, we conducted a study focused on moonless and cloudless nights in Beijing during March–May 2015. Based on VIIRS DNB nighttime data, the BP neural network model is established to monitoring air quality. With the consideration of meteorological elements and the use of spatially and temporally paired data, the accuracy of the proposed BP neural network is improved.

We present data and methods in Section 2, results and discussion in Section 3, and conclusion in Section 4.

2. Data and Methods

2.1. Site Description and Instrumentation

In this paper, 12 $PM_{2.5}$ automatic monitoring sites in Beijing in the spring of 2015 (March–May) are selected as ground-based observation points (as shown in Table 1). The 12 sites, as shown in Figure 1, are located in Beijing (39.4° – 41.6° N, 115.7° – 117.4° E), north China with the typical north temperate semi-humid continental monsoon climate. And this area is featured by a high-temperature rainy summer, cold and dry winter, as well as short-duration spring and autumn. The fine particulate matter $PM_{2.5}$ in Beijing mainly comes from construction dust, industrial emissions, fire coal, biomass burning, secondary aerosol and motor vehicle emission, and can represent the haze pollution in North China. 12 ground monitoring sites selected in this paper are nationally controlled points. As an urban background point, Dingling site in the suburb is located in a topographically open area, with less impact from local circulation, and thus can represent the background situation of ambient air quality of the whole city or even North China region. Three monitoring sites are located in the suburb such as Changping site, Huairou site and Shunyi site. In addition, the remaining 8 monitoring sites located in urban areas are arranged in a small park at an intersection or on a lawn, very close to regions with high density of population, with less human disturbance and desirable air circulation conditions. The monitoring data can reflect the situation of ambient air quality in Beijing effectively.

Table 1. Summary information of the 12 Beijing PM_{2.5} sites.

No.	Site	District	Location	Longitude	Latitude
A	Dingling	Changping	Suburb	116.170	40.287
B	Changping	Changping	Suburb	116.230	40.195
C	Huairou	Huairou	Suburb	116.643	40.394
D	Shunyi	Shunyi	Suburb	116.720	40.144
E	Wanliu	Haidian	Urban	116.315	39.994
F	OlympicCenter	Chaoyang	Urban	116.407	40.003
G	Xigong	Xicheng	Urban	116.366	39.867
H	Tiantan	Dongcheng	Urban	116.434	39.874
I	Dongsi	Dongcheng	Urban	116.434	39.952
J	Nongzhan	Chaoyang	Urban	116.473	39.971
K	Gucheng	Shijingshan	Urban	116.223	39.928
L	Guanyuan	Xicheng	Urban	116.361	39.942

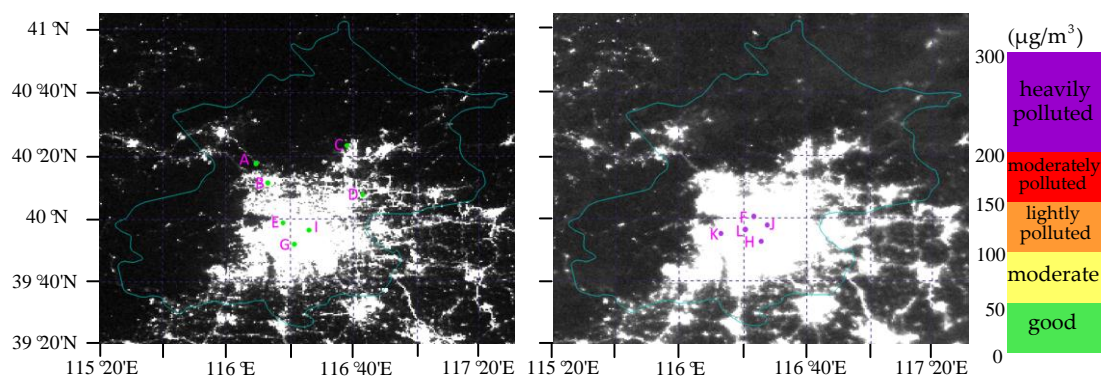


Figure 1. Image of VIIRS DNB radiances for Beijing under different PM_{2.5} concentration.

The above 12 PM_{2.5} automatic monitoring sites adopt the EPA-certified automatic monitor Tapered Element Oscillation Microbalance TEOM1405 F (made by US Thermo) equipped with a Filter dynamics measurement system (FDMS) with a sample cutting diameter of 2.5 µm and a temporal resolution of 1 h. The sampling tube of the automatic monitor equipped with FDMS adopts 30 °C constant temperature heating to dehumidify sampling airflow, so as to make the airflow arriving at the sampling filter dry air. The sampling airflow rate is 1 m³/h, namely, 16.67 L/min. This automatic monitor can determine the decrease in volatile and semi-volatile particulate matter, and gradually correct and compensate determined results to the maximum extent [14].

2.2. Data

2.2.1. PM_{2.5} Mass Concentration Data

The hourly ground observation data of PM_{2.5} mass concentration per day during March–May 2015 can be obtained via the air quality publishing platform of Beijing municipal environmental monitoring center [15].

2.2.2. VIIRS DNB Nighttime Light Data

VIIRS is provided with 22 earth observation channels, including 16 moderate resolution channels (M1–M16) with the nadir spatial resolution of 0.742 km, 5 imaging resolution channels (I1–I5) with the nadir spatial resolution of 0.375 km, and 1 day and night band (DNB) with a nearly constant resolution of 0.742 km across the scan swath. As a low-light detection band, DNB has a broad spectral coverage of 0.4–0.9 µm with a central wavelength of 0.7 µm and a radiation dynamic range up to 10⁷ magnitude (4 × 10^{−9}–3 × 10^{−2}), and can receive weak visible radiation from moonlight, starlight and airglow.

Compared with DMSP-OLS, VIIRS-DNB has been improved in many aspects. In order to realize higher radiation resolution, DNB implements detection by means of dynamic gain, namely, high gain for low radiation scene, medium gain for medium radiation scene, low gain for high radiation scene; the relative radiation gain is up to 119,000:477:1 (high: medium: low gain); the radiation range of each gain mode exceeds 500:1. These three DNB gains (high, medium, low) digitized with 13, 13 and 14-bits [16]. These improvements made to DNB not only avoid the pixel saturation, but also enhance radiation resolution, making DNB still able to detect meteorological and surface features under very weak night illumination conditions, and obtain more clear and accurate nighttime light images.

VIIRS products include data products at different processing levels, i.e., Raw Data Record (RDR), Sensor Data Record (SDR) and Environment Data Record (EDR) [17]. In terms of environmental quantitative monitoring such as city lighting, fire, low stratus, fog, land and sea surface temperature, VIIRS data has shown their tremendous potential. Three types of VIIRS data are used in this paper: (a) VIIRS/DNB SDR data (SVDNB); (b) VIIRS/DNB geographical SDR data (GDNBO); (c) VIIRS/M15 SDR data (SVM15). SVDNB data product provides nighttime light radiation information; GDNBO data product provides corresponding geographical information of longitude, latitude, moon phase angle, moonlight illumination, azimuth and zenith angles of the moon, azimuth and zenith angles for satellite observation; SVM15 data product is used to judge whether there is cloud in the night sky, so as to screen out the cloudless night.

2.2.3. Meteorological Data

Meteorological data such as temperature, dew point temperature, relative humidity, wind speed and atmospheric pressure are measured at Beijing Capital International Airport site. The moon rise and fall time is obtained from CalSKY website [18].

2.3. Method

2.3.1. Theoretical Basic

At night, moonlight and artificial light are two major visible light sources. Artificial light radiation becomes the main light source collected by DNB in the moonless night. The spectra of artificial lights can highly vary, depending on the bulb variety and the color temperature of the light bulb [19]. But the radiances from city lamps are primarily greater than $0.4 \mu\text{m}$ and less than $0.65 \mu\text{m}$ within the. The city light radiation intensity indicates the variation of $\text{PM}_{2.5}$ mass concentration well [12].

We assume that the upward visible radiation from the earth's surface layer is Lambertian [12]. At night, the satellite crosses Beijing at 1:30 am (local time); as after midnight, the intensity and distribution of city lighting are relatively stable. It can be assumed that the radiation intensity of city lighting received by DNB is a constant intensity of I_0 during our three-month study period. Thus, I_0 can be treated as a constant for each location within DNB pixel, but it is varying spatially.

With multiple scattering neglected, the nighttime light radiation intensity I reaching a satellite conforms to Beer's law as shown by the equation:

$$I = I_0 e^{-\tau/\mu} \quad (1)$$

wherein, τ refers to atmospheric optical thickness, and μ is the cosine of satellite viewing angle θ .

The Equation (2) is obtained by sorting out the Equation (1),

$$\tau = \mu \ln(I_0) - \mu \ln(I) \quad (2)$$

wherein, for the pixel of the same location in any image, $\ln(I_0)$ is a constant. Fine particulate matter $\text{PM}_{2.5}$ makes certain contribution to atmosphere optical thickness τ . Assuming the profile of aerosol

extinction coefficient is stable in the nocturnal boundary layer, $PM_{2.5}$ is mixed evenly within an effective height. Therefore, τ can be expressed as follows:

$$\tau = k \times PM_{2.5}^* \quad (3)$$

where k refers to a coefficient, which is related to mass extinction efficiency and aerosol mixing height [12]. Therefore, the Equation (2) can be converted into the Equation (4):

$$PM_{2.5}^* = -A \ln(I) + AB \quad (4)$$

where A is $\frac{h}{k}$, B represents $\ln(I_0)$. Based on radiation transport theory, this equation establishes the relationship between the surface $PM_{2.5}$ mass concentration and the radiation value obtained by DNB. Through multiple regression analysis and statistical analysis, a quantitative inversion model can be set up after meteorological correction.

2.3.2. Models

The cloudy night sky can be removed by use of nighttime VIIRS/M15 band (10.26–11.26 μm) infrared cloud images. By combining ground meteorological information as well as the rising & setting time of moon, the moonless and cloudless night is selected as the sample. Finally, 17 clear nights are screened out from March to May 2015.

(1) Data Preprocessing

Due to a great impact on physical and optical properties of fine particulate matter in the atmosphere by a large amount of water vapor existing in ambient air, the relative humidity factor $f(RH)$ needs to be introduced to correct the humidity of the determined $PM_{2.5}$ mass concentration, so as to enhance its correlativity with radiation intensity of nighttime artificial lights. On the basis of existing experience [20], the $PM_{2.5}$ mass concentration after humidity correction is obtained from the following equation:

$$PM_{2.5}^* = PM_{2.5} \times f(RH) = PM_{2.5} \times \frac{1}{1 - RH/100} \quad (5)$$

wherein, $PM_{2.5}^*$ refers to the $PM_{2.5}$ mass concentration after humidity correction; RH means relative humidity in percentage.

In the selected 17 days as samples, 12 $PM_{2.5}$ automatic monitoring sites carry out continuous monitoring of $PM_{2.5}$ mass concentration each day. Total 198 samples are obtained (missing data excluded). Each sample has 6 input parameters. In this way, network input is a 6-dimensional vector. Due to different dimensions and magnitudes of these data, in order to eliminate dimensions and unify magnitudes, and speed up network computing, a normalized way should be used to input data before network creation. The specific normalization equation is as follows:

$$x_{norm} = 0.5 \times \left(\frac{x - x_{mean}}{x_{max} - x_{min}} \right) + 0.5 \quad (6)$$

wherein, x and x_{norm} refer to values before and after the normalization of input variables respectively; x_{max} and x_{min} are the mean, maximum and minimum values of input variables respectively. In order to ensure that the established model has excellent generalization ability, the number of training sample should be enough large. Therefore, by using random approach, 70% of input data is served as training samples, 15% as test samples and 15% as verification samples.

(2) Model

As VIIRS/DNB radiation data is surface data, in order to precisely match the point data of $PM_{2.5}$ automatic monitoring sites on the point scale, mean of DNB radiance data of 5×5 pixels (approx. 3.7 km \times 3.7 km) around $PM_{2.5}$ automatic monitoring sites could be selected to correspond to surface

measured $PM_{2.5}$. Thus, spatially and temporally paired DNB radiance data, temperature, dew point temperature, relative humidity, atmospheric pressure and wind speed parameters are used as inputs to the model, and surface measured $PM_{2.5}^*$ as model output.

A. Multiple Regression Model

Equation (5) establishes the link between $PM_{2.5}$ concentration and the intensity of lights collected by the VIIRS DNB. The multiple regression based on meteorological elements and the Equation (5), which is based on the radiative transfer theory, can provide a way of $PM_{2.5}$ monitoring.

Leave-one-out cross validation is applied to create the multiple regression model. For each sample, we have 7 sets of known variables (of $PM_{2.5}^*$, DNB radiance data, temperature, dew point temperature, relative humidity, atmospheric pressure and wind speed), the regression analysis can be conducted 198 times. Each time, only 197 sets of variables are used in the regression leaving 1 set of variables out for evaluating the result of regression. For each sample, $PM_{2.5}^*$ is the dependent variable in regression.

B. BP Neural Network Model

In comparison with the general multiple statistical regression, neural network has very superior multivariable nonlinear fitting ability [21]. BP neural network (error back propagation neural network) is most commonly used among neural networks. Its main characteristics are as follows: forward propagation of signals and back propagation of errors. BP neural network has one input layer, one or several hidden layers and one output layer. As theoretically proved, 3-layer network system structure with one hidden layer can approximate any nonlinear problem.

The topological structure of the proposed BP neural network consisted of six neurons in the input layer, one hidden layer with thirteen neurons and one output neuron in the output layer. Thus, the structure of BP neural network can be set as 6-13-1 (as shown in Figure 2). $IW^{1,1}$ is the weight matrix between neurons in input layer and in hidden layer. b^1 is the threshold matrix of neurons in hidden layer. $LW^{2,1}$ is the weight matrix between neurons in hidden layer and in output layer and b^2 is the threshold matrix of neurons in output layer.

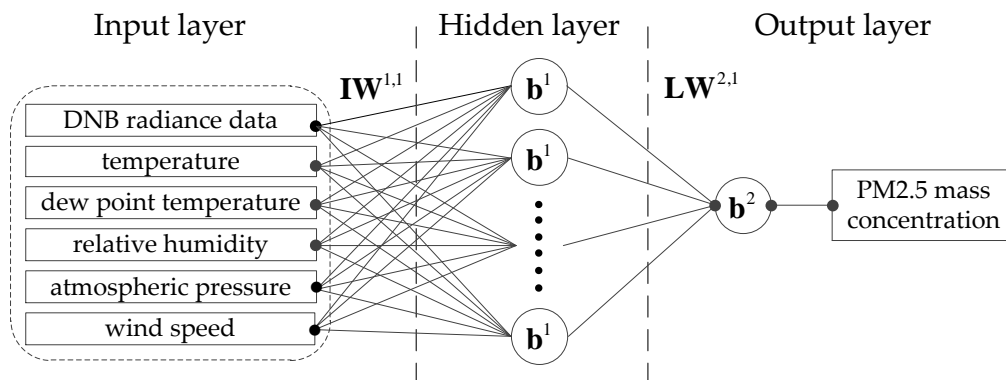


Figure 2. The 6-13-1 topological structure of the BP neuron network model.

After simulation results of BP neural network model are obtained via the aforementioned steps, the Equation (6) is utilized for reverse determination of the variable x ; then $PM_{2.5}$ mass concentration is obtained by reverse normalization of output results.

(3) Model evaluation

Mean bias (MB), normalized mean bias (NMB), normalized mean error (NME) and root mean square error (RMSE) are used as evaluation indexes of model inversion results [22]. MB and RMSE reflect the magnitude of bias and error between the inversion value and measured value; NMB and NME reflect the magnitude of relative bias and error between the inversion value and measured

value; if NMB and NME values are less than 50%, the inversion results of model are good. MB, NMB, NME and RMSE are calculated according to the following equations: $MB = \frac{1}{|N|} \sum_{n \in N} (y_m - y_o)$, $NMB = \frac{\sum_{n \in N} (y_m - y_o)}{\sum_{n \in N} y_o}$, $NME = \frac{\sum_{n \in N} |y_m - y_o|}{\sum_{n \in N} y_o}$, $RMSE = \sqrt{\frac{1}{|N|} \sum_{n \in N} (y_m - y_o)^2}$. In the equation, y_o is the observations and y_m is the result of the inversion model.

To sum up, the inversion of PM_{2.5} mass concentration based on VIIRS/DNB low-light is made by establishing a statistical model between the intensity of nighttime light radiance obtained from VIIRS/DNB and surface measured PM_{2.5} concentration. The specific methods are as follows: (1) NPP satellite and PM_{2.5} auto monitor carry out observation in a synchronized way, and PM_{2.5} auto monitor is utilized to acquire the monitoring values of PM_{2.5} mass concentration at various sites at the time of the satellite crossing; (2) The atmosphere optical thickness (τ) is obtained by the atmospheric radiation transfer theory and light radiance values obtained from VIIRS/DNB; (3) Multiple regression analysis and statistical analysis are conducted on spatially and temporally paired aerosol optical depth and the monitoring values of PM_{2.5}; (4) Through the correction of temperature, dew point temperature, relative humidity, wind speed and atmospheric pressure parameters, the quantitative inversion model of PM_{2.5} mass concentration by DNB is obtained. The inversion flowchart is shown in Figure 3.

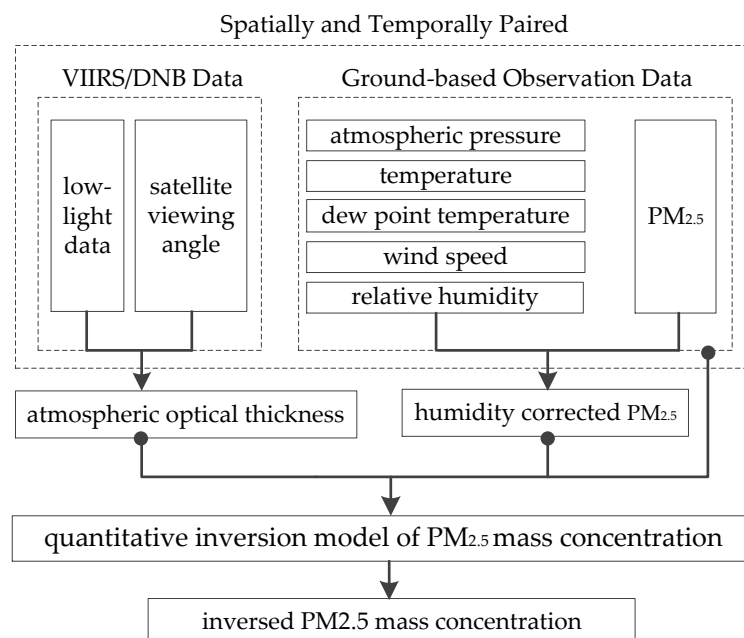


Figure 3. Flow chart of the PM_{2.5} mass concentration inversion model.

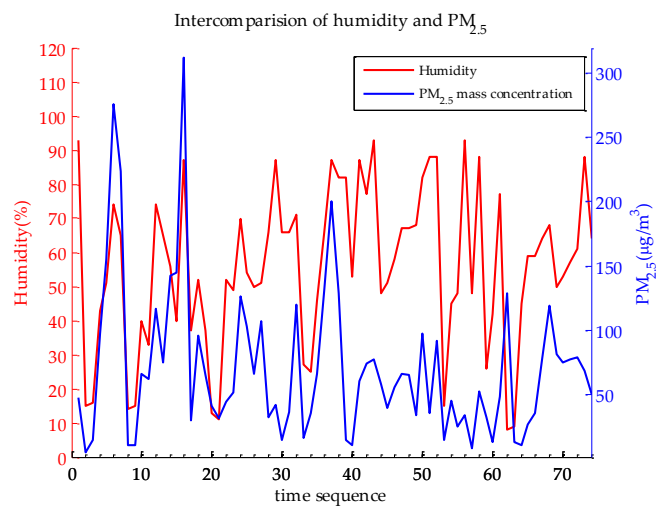
3. Results and Discussion

3.1. Analysis of Meteorological Element

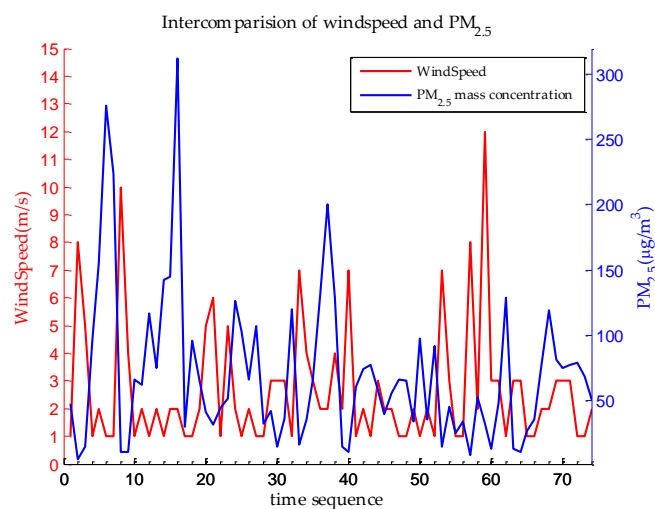
Main factors affecting atmospheric diffusion ability comprise: (1) meteorological dynamics; (2) meteorological thermodynamics. Meteorological dynamics refers to wind and turbulence having a major impact on the diffusion and dilution of pollutants in the atmosphere. Meteorological thermodynamics is involved with temperature stratification and stability [23]. Temperature stratification represents the distribution of temperature with height, and has an impact on the airflow in vertical direction. For example, due to the night thermal inversion layer in spring, vertical convection movement of air is blocked, making atmospheric particulates formed at night difficult to diffuse.

Figure 4 shows the Time sequence diagram of ground-based observed meteorological elements and PM_{2.5} measured by TEOM when the satellite crosses Beijing in the spring (March–May) of

2015. In the figure, vertical coordinates on the left represent the distribution of all meteorological elements (red line); vertical coordinates on the right represent the PM_{2.5} concentration monitoring value (blue line). It can be seen that relative humidity is basically consistent with PM_{2.5} monitoring value in the variation trend, and positive correlation relationship exists between them. When relative humidity is less than 30%, air is generally dry and clean, and PM_{2.5} concentration level is fairly low (below 25 μg/m³). The variation of wind speed is contrary to that of PM_{2.5}. Negative correlation relationship exists between them. At higher wind speed (above 5 m/s), particulate pollutants in the atmosphere can be diffused, making PM_{2.5} mass concentration below 30 μg/m³, and even at 5 μg/m³, hence air quality is fair. At lower wind speed (1–2 m/s), the diffusion of pollutants in the atmosphere is restricted, making PM_{2.5} mass concentration maintained at above 50 μg/m³, and even at 312 μg/m³, and air quality is also bad. Ammonium nitrate (NH₄NO₃) in PM_{2.5} has very strong volatility. Along with temperature rise, NH₄NO₃ is mainly present in the form of HNO₃ and NH₃. Moreover, along with a gradual increase of rainfall in spring, the mean level of PM_{2.5} mass concentration is reduced to some extent, and events of heavy pollution are relatively decreased, which is related to active airflow exchange after temperature increase as well as stopped heating in Beijing during April and May.



(a)



(b)

Figure 4. Cont.

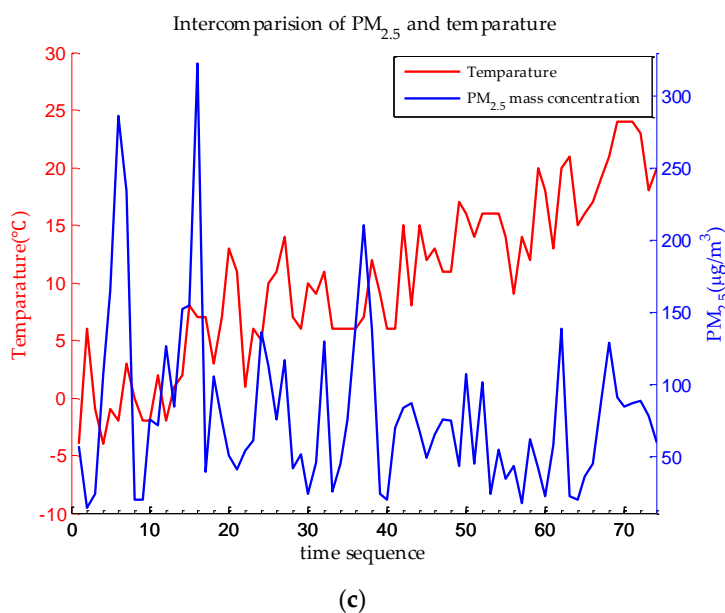


Figure 4. Time sequence diagram of various nighttime meteorological elements and PM_{2.5} concentration monitoring value in Beijing in Spring. (a) Time sequence diagram of relative humidity and PM_{2.5} concentration monitoring value; (b) Time sequence diagram of wind speed and PM_{2.5} concentration monitoring value; (c) Time sequence diagram of temperature and PM_{2.5} concentration monitoring value.

Based on the above analysis, it can be preliminarily seen that dust-haze is generally accompanied by appropriate relative humidity (60%–85%), calm wind or small wind (1 m/s–2 m/s). The time of satellite crossing is at about 2:00 a.m.; radiation temperature drop makes humidity obviously increased; thus, the relative humidity collected at this time is maintained at a high level. It is clear that each meteorological element has a certain impact on PM_{2.5} mass concentration, so it should be taken into consideration during the establishment of the quantitative model.

3.2. Model Verification

198 sample sets are utilized to build the multiple regression model and BP neural network model respectively. According to leave-one-out cross validation, the inversion value of PM_{2.5} mass concentration is obtained, and compared with the actual monitoring value of PM_{2.5} and analyzed for the evaluation of these models. As seen from Table 2, MB, NMB, NME and RMSE of inversion results of BP neural network model are 0.17 µg/m³, 0.29%, 16% and 14.02 µg/m³ respectively, which are all superior to inversion results of the multiple regression model (10.71 µg/m³, 18%, 62%, 46.03 µg/m³). It illustrates that inversion results of the BP neural network model are more accurate.

Table 2. Model evaluation.

	MB	NMB	NME	RMSE
Multiple regression model	10.71	18%	62%	46.03
BP neural network model	0.17	0.29%	16%	14.02

Inversion results of the BP neural network model are further compared with actual results. Figure 5 shows the comparison of PM_{2.5} mass concentration inverted by the BP neural network model and ground monitoring value. In Figure 5a, the dash line represents a datum line with a slope of 1, and the solid line is the fitting curve of the predicted PM_{2.5} and measured PM_{2.5}. The magnitude of

slope value of the fitting curve represents the closeness of the predicted value and measured value of PM_{2.5} mass concentration; the bigger the slope value is, the closer the predicted result is to the measured value. It can be seen that the comparison of PM_{2.5} mass concentration (X) predicted by the BP neural network model with the measured value (Y) shows quite high linear correlation with the correlation coefficient R of 0.91, and the linear fitting equation $Y = 0.9952X + 0.1096$. As seen from the sample sequence comparison of Figure 5b, the overall bias in the inversion results is close to zero (Mean ± Standard Deviation of X : 59.399 ± 30.175 and Y : 59.222 ± 33.141), and they basically keep the consistent variation trend. Such results indicate that the PM_{2.5} mass concentration predicted by the BP neural network model has certain credibility and accuracy.

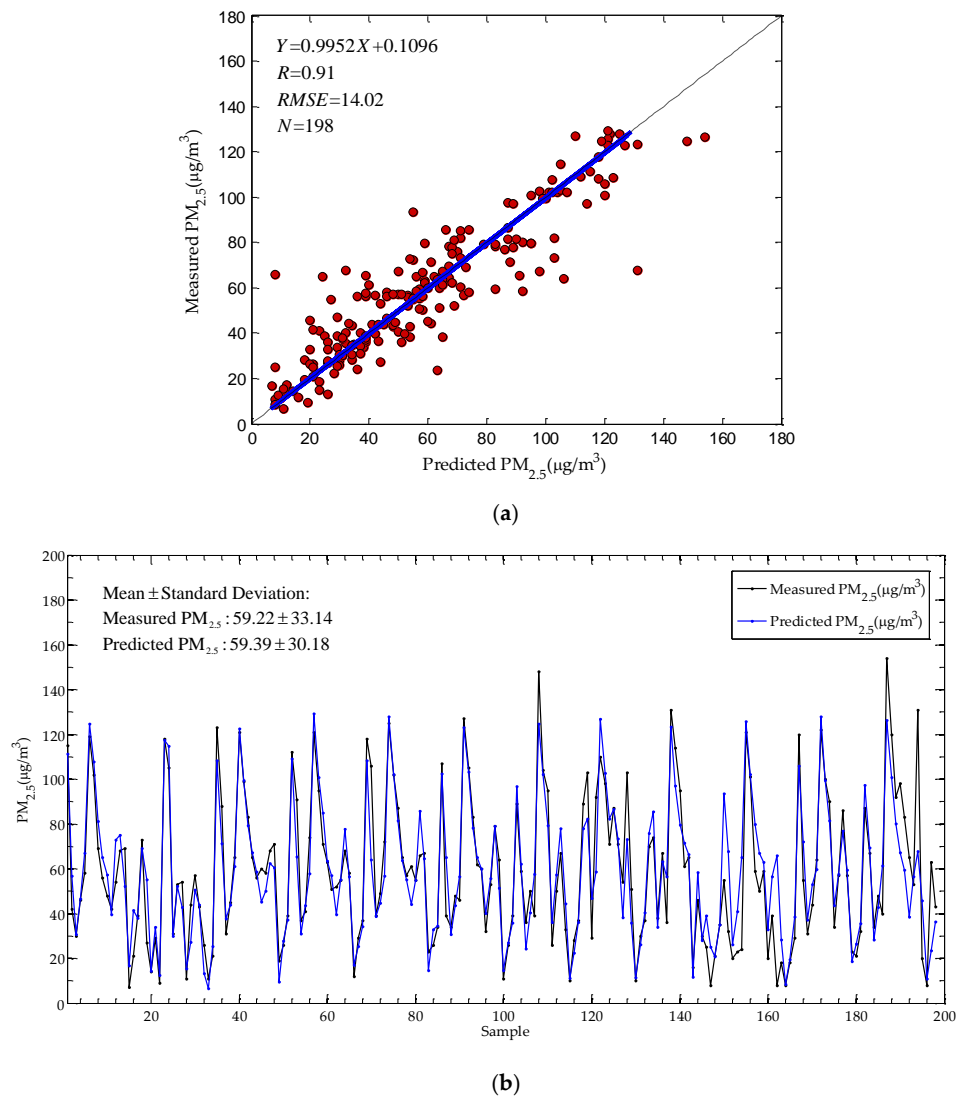


Figure 5. Comparison of PM_{2.5} mass concentration values inverted by the BP neural network model and TEOM1405F monitoring values.

3.3. Relative Humidity Impact Analysis

Figure 6 shows comparison results of inversion values and TEOM1405F monitoring values of PM_{2.5} mass concentration under different relative humidity (RH) conditions, with linear fitting and correlation analysis made. As indicated by the results, when the relative humidity in the range of 40% to 80%, the correlation coefficient between PM_{2.5} mass concentration predicted by the model and measured by TEOM1405F is above 0.8; but when the relative humidity is less than 40% or greater

than 80%, the predicted $PM_{2.5}$ has a slightly larger difference with measured $PM_{2.5}$. Cause analysis: when the relative humidity is less than 40%, the air is generally dry and clean, and the concentration level of $PM_{2.5}$ is low, causing unobvious attenuation of visible light by rare particulates, making the variation of visible light radiation obtained through DNB also unobvious, and reducing the sensitivity of the BP neural network model, as a result, reducing the correlation of inversion results. When the relative humidity is more than 80%, due to reinforced attenuation of visible light by water vapor, the attenuation of visible light by particulates is weakened, resulting in a bigger error of inversion results and thus a larger difference with monitoring results. However, due to insufficient monitoring data under different relative humidity conditions, the study on the impact of relative humidity on inversion results still needs more observation data for analysis.

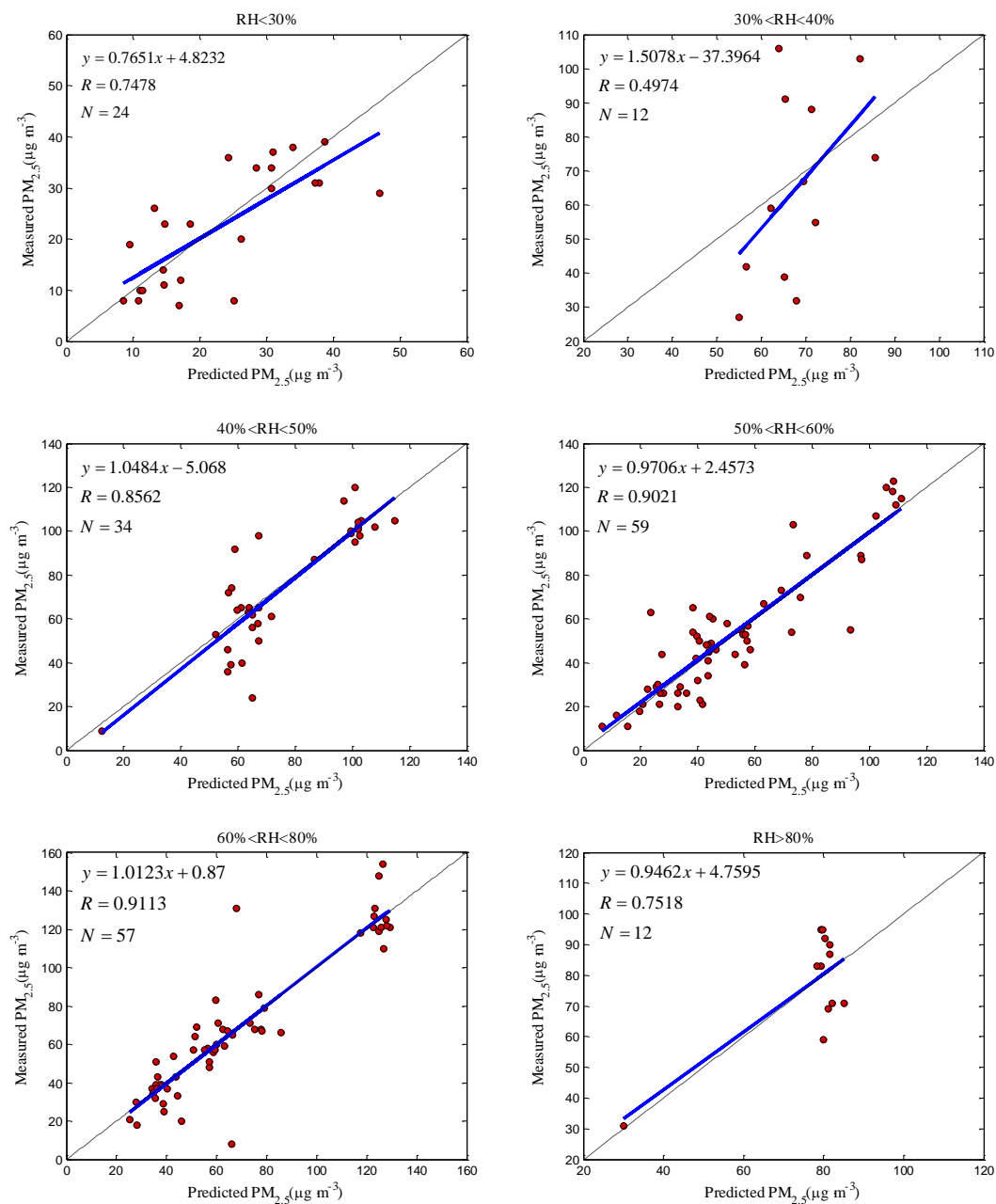


Figure 6. Correlation between $PM_{2.5}$ mass concentration predicted by the BP neural network model and measured by TEOM1405F as classified according to different relative humidity.

3.4. Influence of PM_{2.5} Concentration on the Application Scope of BP Neural Network Model

Based on the BP neural network approach, PM_{2.5} mass concentration values inverted by DNB at night have good consistency with measured values, but this model is somewhat limited during inversion. This paper carries out comparative analysis of PM_{2.5} mass concentration values inverted by the BP neural network model (predicted values) and PM_{2.5} mass concentration monitored by TEOM1405F (measured values). Deviation rate is defined as

$$\text{Deviation rate} = \frac{\text{predicted values} - \text{measured values}}{\text{measured values}} \quad (7)$$

Figure 7 is the comparison diagram of PM_{2.5} mass concentration values inverted by the BP neural network model and TEOM1405F monitoring values. In the figure, the red represents ± 0.5 times of deviation. Clearly, when PM_{2.5} mass concentration is less than 40 $\mu\text{g}/\text{m}^3$, inversion results have a bigger difference from the values measured by the automatic monitor, and the maximum deviation rate is up to 8. However, when PM_{2.5} mass concentration is more than 40 $\mu\text{g}/\text{m}^3$, the deviation rate is basically controlled between two red lines, i.e., within ± 0.5 times. Therefore, when PM_{2.5} mass concentration in the atmosphere is less than 40 $\mu\text{g}/\text{m}^3$, it is not recommended to use this method for PM_{2.5} detection.

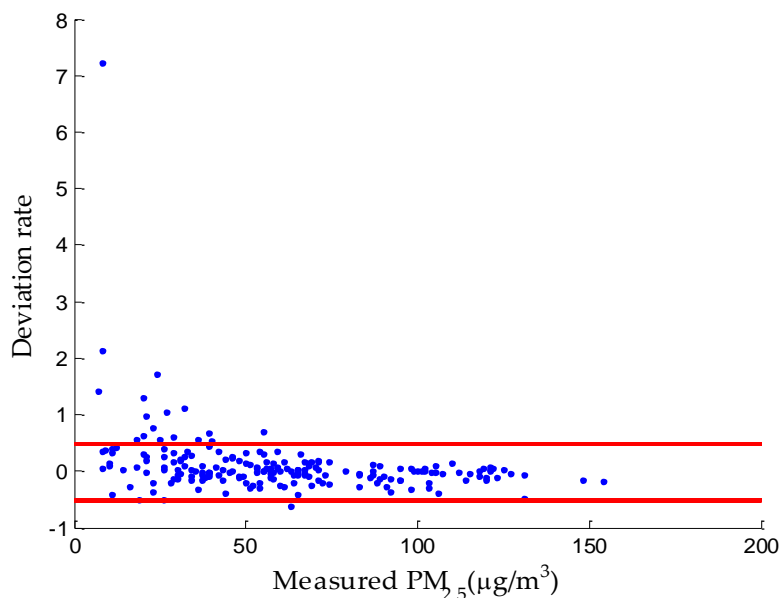


Figure 7. Deviation rate of predicted PM_{2.5}.

Issues to be optimized in the future work: (i) Human activities mainly occur in the early half of the night, while NPP satellite crosses Beijing in the later half of the night. Therefore, ground artificial light source as background light source is stable, and it can be assumed that background light intensity is unvarying. However, within a 3-month time scale, it is unavoidable for background light source to vary. The further work is to get rid of effects brought by the variation of background light source through making background base images; (ii) According to infrared images of VIIRS/M15, it is very difficult to distinguish low clouds, thin clouds and heavy fog. In the moonless night, the weakening of light by low clouds, thin clouds and heavy fog is close to the weakening of light by aerosol particles, and their presence will affect inversion accuracy. The judgment of low clouds, thin clouds and heavy fog needs to depend on more NPP/VIIRS cloud detection production; (iii) With regard to the mixed-layer height of aerosol, because it is impossible to carry out real-time onsite measurement, this paper assumes that the profile of aerosol extinction coefficients of nighttime boundary layer is stable, and the mixed-layer

height of aerosol is processed as a constant. In the future work, this processing method for the mixed-layer height of aerosol will be improved once observation data of this element is obtained.

4. Conclusions

In this study, based on the radiative transfer theory, we establish the inversion model of nighttime $PM_{2.5}$ concentration by using VIIRS/DNB low-light data. The main conclusions can be summarized as follows:

The study focused on the moonless and cloudless nights in Beijing during March–May 2015. The ground-based observation shows that, during the 3-month period, the dust-haze is generally accompanied by appropriate relative humidity (60%–85%), calm wind or small wind (1 m/s–2 m/s). Spatially and temporally paired elements such as DNB data, temperature, dew point temperature, relative humidity, atmospheric pressure and wind speed are considered to establish the multiple regression inversion model and BP neural network inversion model respectively. The MB, NMB, NME and RMSE of the BP neural network model are 0.17 $\mu\text{g}/\text{m}^3$, 0.29%, 16%, 14.02 $\mu\text{g}/\text{m}^3$ respectively, while them of the multiple regression model respectively are 10.71 $\mu\text{g}/\text{m}^3$, 18%, 62%, 46.03 $\mu\text{g}/\text{m}^3$, which shows the BP neural network model are superior to the multiple regression model. And the linear correlation coefficient (R) between inversion results of the BP neural network model and the corresponding measured $PM_{2.5}$ is 0.91, and the RMSE is 14.02 $\mu\text{g}/\text{m}^3$ with the average of 59.39 $\mu\text{g}/\text{m}^3$. The analysis of BP neural network model sensitivity suggests that the model is more accurate when the relative humidity is 40%–80% and ground $PM_{2.5}$ mass concentration exceeds 40 $\mu\text{g}/\text{m}^3$.

The main innovation of this study is presented as follows. The meteorological elements is firstly introduced to the inversion model to improve the accuracy. And spatially and temporally paired data of ground-based and satellite observation are used to create the inversion model to ensure the facticity of the model. In addition, we use the mean of DNB radiance data of 5×5 pixels (approx. 3.7 km \times 3.7 km) around ground-based $PM_{2.5}$ automatic monitoring sites to correspond the $PM_{2.5}$ mass concentration in order to make the areal data of DNB match the point data of $PM_{2.5}$ well.

The establishment of the BP neural network model for $PM_{2.5}$ mass concentration provides a feasibility reference for further large-scale monitoring of the spatial distribution of $PM_{2.5}$ concentration and improvement of assessment methods for nighttime air quality in the city.

Supplementary Materials: The following are available online at <http://www.mdpi.com/2073-4433/7/10/136/s1>, Figure S1: Structure of BP Neural Network.

Acknowledgments: This work is financially supported by National Natural Science Foundation of China (41375028 and 41576171).

Author Contributions: Xiaoran Zhao wrote the article; Hanqing Shi and Hong Yu conceived and designed the experiments; Xiaoran Zhao and Pinglv Yang performed the experiments; Pinglv Yang analyzed the data.

Conflicts of Interest: The authors declare no conflict of interest.

References

1. Chow, J.C.; Watson, J.G. *Guideline on Speciated Particulate Monitoring*; Report Prepared for U.S. Environmental Protection Agency, Research Triangle Park, NC, USA; Desert Research Institute: Reno, NV, USA, 1998.
2. Yang, F.M.; Ma, Y.L.; He, K.B. A brief introduction to $PM_{2.5}$ and related research. *World Environ.* **2000**, *2000*, 32–34.
3. Gomišček, B.; Hauck, H.; Stopper, S.; Preining, O. Spatial and temporal variations of PM_1 , $PM_{2.5}$, PM_{10} and particle number concentration during the AUPHEP—Project. *Atmos. Environ.* **2004**, *38*, 3917–3934. [[CrossRef](#)]
4. Lee, H.J.; Liu, Y.; Coull, B.A.; Schwartz, J.; Koutrakis, P. A novel calibration approach of MODIS AOD data to predict $PM_{2.5}$ concentration. *Atmos. Chem. Phys. Discuss.* **2011**, *11*, 9769–9795. [[CrossRef](#)]
5. Van Donkelaar, A.; Martin, R.V.; Park, R.J. Estimating ground-level $PM_{2.5}$ using aerosol optical depth determined from satellite remote sensing. *J. Geophys. Res. Atmos.* **2006**. [[CrossRef](#)]

6. Guo, H.; Cheng, T.H.; Gu, X.F.; Chen, H.; Wang, Y.; Zheng, F.; Xiang, K. Comparison of four ground-level PM_{2.5} estimation models using PARASOL aerosol optical depth data from China. *Int. J. Environ. Res. Public Health* **2016**. [[CrossRef](#)] [[PubMed](#)]
7. Miller, S.D.; Mills, S.P.; Elvidge, C.D.; Lindsey, D.T.; Lee, T.F.; Hawkins, J.D. Suomi satellite brings to light a unique frontier of nighttime environmental sensing capabilities. *Proc. Natl. Acad. Sci. USA* **2012**, *109*, 15706–15711. [[CrossRef](#)] [[PubMed](#)]
8. Lee, T.E.; Miller, S.D.; Turk, F.J.; Schueler, C.; Julian, R.; Deyo, S.; Dills, P.; Wang, S. The NPOESS VIIRS day/night visible sensor. *Bull. Am. Meteorol. Soc.* **2006**, *87*, 191–199. [[CrossRef](#)]
9. Chow, J.C.; Watson, J.G.; Fujita, E.M.; Lu, Z.; Lawson, D.R.; Ashbaugh, L.L. Temporal and spatial variations of PM_{2.5} and PM₁₀ aerosol in the Southern California air quality study. *Atmos. Environ.* **1994**, *28*, 2061–2080. [[CrossRef](#)]
10. Zhao, X.J.; Zhang, X.L.; Xu, X.F.; Fujita, E.M.; Lu, Z.; Lawson, D.R.; Ashbaugh, L.L. Seasonal and diurnal variations of ambient PM_{2.5} concentration in urban and rural environment in Beijing. *Atmos. Environ.* **2009**, *43*, 2893–2900. [[CrossRef](#)]
11. Chow, J.C.; Watson, J.G. Review of PM_{2.5} and PM₁₀ apportionment for fossil fuel combustion and other sources by the chemical mass balance receptor model. *Energy Fuels* **2002**, *16*, 222–260. [[CrossRef](#)]
12. Wang, J.; Aegerter, C.; Xu, X.; Szykman, J.J. Potential application of VIIRS Day/Night Band for monitoring nighttime surface PM_{2.5} air quality from space. *Atmos. Environ.* **2016**, *124*, 55–63. [[CrossRef](#)]
13. Li, R.; Liu, X.; Li, X. Estimation of the PM_{2.5} pollution levels in Beijing based on nighttime light data from the defense meteorological satellite program-operational linescan system. *Atmosphere* **2015**, *6*, 607–622. [[CrossRef](#)]
14. Allen, G.; Sioutas, C.; Koutraki, P.; Reiss, R.; Lurmann, F.W.; Roberts, P.T. Evaluation of the TEOM[®] method for measurement of ambient particulate mass in urban areas. *J. Air Waste Manag. Assoc.* **1997**, *47*, 682–689. [[CrossRef](#)] [[PubMed](#)]
15. Beijing municipal environmental monitoring center. Available online: <http://www.bjmemc.com.cn> (accessed on 14 October 2016).
16. Elvidge, C.D.; Baugh, K.E.; Zhizhin, M.; Hsu, F.C. Why VIIRS data are superior to DMSP for mapping nighttime lights. *Proc. Asia-Pac. Adv. Netw.* **2013**, *35*, 62–69. [[CrossRef](#)]
17. Liu, Q.; Cao, C.; Wang, F. Assessment of Suomi National Polar-Orbiting Partnership VIIRS emissive band calibration and inter-sensor comparisons. *IEEE J. Sel. Top. Appl. Earth Obs. Remote Sens.* **2013**, *6*, 1737–1748. [[CrossRef](#)]
18. CalSKY. Available online: <http://www.calsky.com> (accessed on 14 October 2016).
19. Elvidge, C.D.; Keith, D.M.; Tuttle, B.T.; Baugh, K.E. Spectral identification of lighting type and character. *Sensors* **2010**, *10*, 3961–3988. [[CrossRef](#)] [[PubMed](#)]
20. Zhang, J.; Reid, J.S.; Miller, S.D.; Turk, F.J. Strategy for studying nocturnal aerosol optical depth using artificial lights. *Int. J. Remote Sens.* **2008**, *29*, 4599–4613. [[CrossRef](#)]
21. Li, C.C.; Mao, J.T.; Lau, A.K.; Yuan, Z.B.; Wang, M.H.; Liu, X.Y. Application of MODIS satellite product to the air pollution research in Beijing. *Sci. China Ser. D* **2005**, *35*, 177–186.
22. An, X.Q.; Zhu, T.; Wang, Z.F.; Li, C.Y.; Wang, Y.S. A modeling analysis of a heavy air pollution episode occurred in Beijing. *Atmos. Chem. Phys.* **2007**, *7*, 3103–3114. [[CrossRef](#)]
23. Yao, X.; Chan, C.K.; Fang, M.; Cadle, S.; Chan, T.; Mulawa, P.; He, K.; Ye, B. The water-soluble ionic composition of PM_{2.5} in Shanghai and Beijing, China. *Atmos. Environ.* **2002**, *36*, 4223–4234. [[CrossRef](#)]

